Published for SISSA by Springer

Received: May 10, 2013
Accepted: June 26, 2013
Published: July 11, 2013

Differential branching fraction and angular analysis of the decay $B_s^0 \to \phi\mu^+\mu^-$

The LHCb collaboration

E-mail: christoph.langenbruch@cern.ch

Abstract: The determination of the differential branching fraction and the first angular analysis of the decay $B_s^0 \to \phi\mu^+\mu^-$ are presented using data, corresponding to an integrated luminosity of $1.0\,\text{fb}^{-1}$, collected by the LHCb experiment at $\sqrt{s} = 7\,\text{TeV}$. The differential branching fraction is determined in bins of q^2, the invariant dimuon mass squared. Integration over the full q^2 range yields a total branching fraction of $\mathcal{B}(B_s^0 \to \phi\mu^+\mu^-) = \left(7.07\,^{+0.64}_{-0.59} \pm 0.17 \pm 0.71\right) \times 10^{-7}$, where the first uncertainty is statistical, the second systematic, and the third originates from the branching fraction of the normalisation channel. An angular analysis is performed to determine the angular observables F_L, S_3, A_6, and A_9. The observables are consistent with Standard Model expectations.

Keywords: Rare decay, Hadron-Hadron Scattering, B physics, Flavor physics

ArXiv ePrint: 1305.2168

Open Access, Copyright CERN,
for the benefit of the LHCb collaboration

doi:10.1007/JHEP07(2013)084

JHEP07(2013)084

Contents

JHEP07(2013)084

1 Introduction

The $B_s^0 \to \phi\mu^+\mu^-$ ($\phi \to K^+K^-$) decay[1] involves a $b \to s$ quark transition and therefore constitutes a flavour changing neutral current (FCNC) process. Since FCNC processes are forbidden at tree level in the Standard Model (SM), the decay is mediated by higher order (box and penguin) diagrams. In scenarios beyond the SM new particles can affect both the branching fraction of the decay and the angular distributions of the decay products.

The angular configuration of the $K^+K^-\mu^+\mu^-$ system is defined by the decay angles θ_K, θ_ℓ, and Φ. Here, θ_K (θ_ℓ) denotes the angle of the K^- (μ^-) with respect to the direction of flight of the B_s^0 meson in the K^+K^- ($\mu^+\mu^-$) centre-of-mass frame, and Φ denotes the relative angle of the $\mu^+\mu^-$ and the K^+K^- decay planes in the B_s^0 meson centre-of-mass frame [1]. In contrast to the decay $B^0 \to K^{*0}\mu^+\mu^-$, the final state of the decay $B_s^0 \to \phi\mu^+\mu^-$ is not flavour specific. The differential decay rate, depending on the decay angles and the invariant mass squared of the dimuon system is given by

$$\begin{aligned}\frac{1}{\mathrm{d}\Gamma/\mathrm{d}q^2}\frac{\mathrm{d}^4\Gamma}{\mathrm{d}q^2\mathrm{d}\cos\theta_\ell\mathrm{d}\cos\theta_K\mathrm{d}\Phi} = \frac{9}{32\pi}\big[&S_1^s\sin^2\theta_K + S_1^c\cos^2\theta_K \\ &+S_2^s\sin^2\theta_K\cos 2\theta_\ell + S_2^c\cos^2\theta_K\cos 2\theta_\ell \\ &+S_3\sin^2\theta_K\sin^2\theta_\ell\cos 2\Phi + S_4\sin 2\theta_K\sin 2\theta_\ell\cos\Phi \\ &+A_5\sin 2\theta_K\sin\theta_\ell\cos\Phi + A_6\sin^2\theta_K\cos\theta_\ell \\ &+S_7\sin 2\theta_K\sin\theta_\ell\sin\Phi + A_8\sin 2\theta_K\sin 2\theta_\ell\sin\Phi \\ &+A_9\sin^2\theta_K\sin^2\theta_\ell\sin 2\Phi\big],\end{aligned} \tag{1.1}$$

[1] The inclusion of charge conjugated processes is implied throughout this paper.

where equal numbers of produced B_s^0 and $\overline{B}_s^0$ mesons are assumed [2]. The q^2-dependent angular observables $S_i^{(s,c)}$ and A_i correspond to CP averages and CP asymmetries, respectively. Integrating eq. (1.1) over two angles, under the assumption of massless leptons, results in three distributions, each depending on one decay angle

$$\frac{1}{\mathrm{d}\Gamma/\mathrm{d}q^2}\frac{\mathrm{d}^2\Gamma}{\mathrm{d}q^2\,\mathrm{d}\cos\theta_K} = \frac{3}{4}(1-F_{\mathrm{L}})(1-\cos^2\theta_K) + \frac{3}{2}F_{\mathrm{L}}\cos^2\theta_K, \tag{1.2}$$

$$\frac{1}{\mathrm{d}\Gamma/\mathrm{d}q^2}\frac{\mathrm{d}^2\Gamma}{\mathrm{d}q^2\,\mathrm{d}\cos\theta_\ell} = \frac{3}{8}(1-F_{\mathrm{L}})(1+\cos^2\theta_\ell) + \frac{3}{4}F_{\mathrm{L}}(1-\cos^2\theta_\ell) + \frac{3}{4}A_6\cos\theta_\ell, \tag{1.3}$$

$$\frac{1}{\mathrm{d}\Gamma/\mathrm{d}q^2}\frac{\mathrm{d}^2\Gamma}{\mathrm{d}q^2\,\mathrm{d}\Phi} = \frac{1}{2\pi} + \frac{1}{2\pi}S_3\cos 2\Phi + \frac{1}{2\pi}A_9\sin 2\Phi, \tag{1.4}$$

which retain sensitivity to the angular observables $F_{\mathrm{L}}(=S_1^c=-S_2^c)$, S_3, A_6, and A_9. Of particular interest is the T-odd asymmetry A_9 where possible large CP-violating phases from contributions beyond the SM would not be suppressed by small strong phases [1].

This paper presents a measurement of the differential branching fraction and the angular observables F_{L}, S_3, A_6, and A_9 in six bins of q^2. In addition, the total branching fraction is determined. The data used in the analysis were recorded by the LHCb experiment in 2011 in pp collisions at $\sqrt{s} = 7\,\mathrm{TeV}$ and correspond to an integrated luminosity of $1.0\,\mathrm{fb}^{-1}$.

2 The LHCb detector

The LHCb detector [3] is a single-arm forward spectrometer covering the pseudorapidity range $2 < \eta < 5$, designed for the study of particles containing b or c quarks. The detector includes a high precision tracking system consisting of a silicon-strip vertex detector surrounding the pp interaction region, a large-area silicon-strip detector located upstream of a dipole magnet with a bending power of about 4 Tm, and three stations of silicon-strip detectors and straw drift tubes placed downstream. The combined tracking system provides a momentum measurement with relative uncertainty that varies from 0.4% at $5\,\mathrm{GeV}/c$ to 0.6% at $100\,\mathrm{GeV}/c$, and impact parameter (IP) resolution of $20\,\mu\mathrm{m}$ for tracks with high transverse momentum. Charged hadrons are identified using two ring-imaging Cherenkov detectors. Photon, electron and hadron candidates are identified by a calorimeter system consisting of scintillating-pad and preshower detectors, an electromagnetic calorimeter and a hadronic calorimeter. Muons are identified by a system composed of alternating layers of iron and multiwire proportional chambers. The LHCb trigger system [4] consists of a hardware stage, based on information from the calorimeter and muon systems, followed by a software stage which applies a full event reconstruction.

Simulated signal event samples are generated to determine the trigger, reconstruction and selection efficiencies. Exclusive samples are analysed to estimate possible backgrounds. The simulation generates pp collisions using Pythia 6.4 [5] with a specific LHCb configuration [6]. Decays of hadronic particles are described by EvtGen [7] in which final state radiation is generated using Photos [8]. The interaction of the generated particles with the detector and its response are implemented using the Geant4 toolkit [9, 10] as described

JHEP07(2013)084

in ref. [11]. Data driven corrections are applied to the simulated events to account for differences between data and simulation. These include the IP resolution, tracking efficiency, and particle identification performance. In addition, simulated events are reweighted depending on the transverse momentum ($p_{\rm T}$) of the B_s^0 meson, the vertex fit quality, and the track multiplicity to match distributions of control samples from data.

3 Selection of signal candidates

Signal candidates are accepted if they are triggered by particles of the $B_s^0 \to \phi\mu^+\mu^-$ ($\phi \to K^+K^-$) final state. The hardware trigger requires either a high transverse momentum muon or muon pair, or a high transverse energy ($E_{\rm T}$) hadron. The first stage of the software trigger selects events containing a muon (or hadron) with $p_{\rm T} > 0.8\,{\rm GeV}/c$ ($E_{\rm T} > 1.5\,{\rm GeV}/c$) and a minimum IP with respect to all primary interaction vertices in the event of 80 μm (125 μm). In the second stage of the software trigger the tracks of two or more final state particles are required to form a vertex that is significantly displaced from all primary vertices (PVs) in the event.

Candidates are selected if they pass a loose preselection that requires the kaon and muon tracks to have a large $\chi^2_{\rm IP}$ (> 9) with respect to the PV. The $\chi^2_{\rm IP}$ is defined as the difference between the χ^2 of the PV reconstructed with and without the considered particle. The four tracks forming a B_s^0 candidate are fit to a common vertex, which is required to be of good quality ($\chi^2_{\rm vtx} < 30$) and well separated from the PV ($\chi^2_{\rm FD} > 121$, where FD denotes the flight distance). The angle between the B_s^0 momentum vector and the vector connecting the PV with the B_s^0 decay vertex is required to be small. Furthermore, B_s^0 candidates are required to have a small IP with respect to the PV ($\chi^2_{\rm IP} < 16$). The invariant mass of the K^+K^- system is required to be within $12\,{\rm MeV}/c^2$ of the known ϕ mass [12].

To further reject combinatorial background events, a boosted decision tree (BDT) [13] using the AdaBoost algorithm [14] is applied. The BDT training uses $B_s^0 \to J/\psi\,\phi$ ($J/\psi \to \mu^+\mu^-$) candidates as proxy for the signal, and candidates in the $B_s^0 \to \phi\mu^+\mu^-$ mass sidebands ($5100 < m(K^+K^-\mu^+\mu^-) < 5166\,{\rm MeV}/c^2$ and $5566 < m(K^+K^-\mu^+\mu^-) < 5800\,{\rm MeV}/c^2$) as background. The input variables of the BDT are the $\chi^2_{\rm IP}$ of all final state tracks and of the B_s^0 candidate, the angle between the B_s^0 momentum vector and the vector between PV and B_s^0 decay vertex, the vertex fit χ^2, the flight distance significance and transverse momentum of the B_s^0 candidate, and particle identification information of the muons and kaons in the final state.

Several types of b-hadron decays can mimic the final state of the signal decay and constitute potential sources of peaking background. The resonant decays $B_s^0 \to J/\psi\,\phi$ and $B_s^0 \to \psi(2S)\phi$ with $\psi(2S) \to \mu^+\mu^-$ are rejected by applying vetoes on the dimuon mass regions around the charmonium resonances, $2946 < m(\mu^+\mu^-) < 3176\,{\rm MeV}/c^2$ and $3592 < m(\mu^+\mu^-) < 3766\,{\rm MeV}/c^2$. To account for the radiative tails of the charmonium resonances the vetoes are enlarged by $200\,{\rm MeV}/c^2$ to lower $m(\mu^+\mu^-)$ for reconstructed B_s^0 masses below $5316\,{\rm MeV}/c^2$. In the region $5416 < m(B_s^0) < 5566\,{\rm MeV}/c^2$ the vetoes are extended by $50\,{\rm MeV}/c^2$ to higher $m(\mu^+\mu^-)$ to reject a small fraction of J/ψ and $\psi(2S)$ decays that are misreconstructed at higher masses. The decay $B^0 \to K^{*0}\mu^+\mu^-$ ($K^{*0} \to K^+\pi^-$) can be

JHEP07(2013)084

reconstructed as signal if the pion is misidentified as a kaon. This background is strongly suppressed by particle identification criteria. In the narrow ϕ mass window, 2.4 ± 0.5 misidentified $B^0 \to K^{*0}\mu^+\mu^-$ candidates are expected within $\pm 50\,\mathrm{MeV}/c^2$ of the known B_s^0 mass of $5366\,\mathrm{MeV}/c^2$ [12]. The resonant decay $B_s^0 \to J/\psi\,\phi$ can also constitute a source of peaking background if the K^+ (K^-) is misidentified as μ^+ (μ^-) and vice versa. Similarly, the decay $B^0 \to J/\psi\,K^{*0}$ ($K^{*0} \to K^+\pi^-$) where the π^- (μ^-) is misidentified as μ^- (K^-) can mimic the signal decay. These backgrounds are rejected by requiring that the invariant mass of the $K^+\mu^-$ ($K^-\mu^+$) system, with kaons reconstructed under the muon mass hypothesis, is not within $\pm 50\,\mathrm{MeV}/c^2$ around the known J/ψ mass of $3096\,\mathrm{MeV}/c^2$ [12], unless both the kaon and the muon pass stringent particle identification criteria. The expected number of background events from double misidentification in the B_s^0 signal mass region is 0.9 ± 0.5. All other backgrounds studied, including semileptonic $b \to c\,\mu^-\bar{\nu}_\mu(c \to s\,\mu^+\nu_\mu)$ cascades, hadronic double misidentification from $B_s^0 \to D_s^-\pi^+(D_s^- \to \phi\pi^-)$, and the decay $\Lambda_b^0 \to \Lambda(1520)\,\mu^+\mu^-$, have been found to be negligible.

4 Differential branching fraction

Figure 1 shows the $\mu^+\mu^-$ versus the $K^+K^-\mu^+\mu^-$ invariant mass of the selected candidates. The signal decay $B_s^0 \to \phi\mu^+\mu^-$ is clearly visible in the B_s^0 signal region. The determination of the differential branching fraction is performed in six bins of q^2, given in table 1, and corresponds to the binning chosen for the analysis of the decay $B^0 \to K^{*0}\mu^+\mu^-$ [15]. Figure 2 shows the $K^+K^-\mu^+\mu^-$ mass distribution in the six q^2 bins. The signal yields are determined by extended unbinned maximum likelihood fits to the reconstructed B_s^0 mass distributions. The signal component is modeled by a double Gaussian function. The resolution parameters are obtained from the resonant $B_s^0 \to J/\psi\,\phi$ decay. A q^2-dependent scaling factor, determined with simulated $B_s^0 \to \phi\mu^+\mu^-$ events, is introduced to account for the observed q^2 dependence of the mass resolution. The combinatorial background is described by a single exponential function. The veto of the radiative tails of the charmonium resonances is accounted for by using a scale factor. The resulting signal yields are given in table 1. Fitting for the signal yield over the full q^2 region, 174 ± 15 signal candidates are found. A fit of the normalisation mode $B_s^0 \to J/\psi\,\phi$ yields $(20.36 \pm 0.14) \times 10^3$ candidates.

The differential branching fraction of the signal decay in the q^2 interval spanning from q^2_{min} to q^2_{max} is calculated according to

$$\frac{\mathrm{d}\mathcal{B}(B_s^0 \to \phi\mu^+\mu^-)}{\mathrm{d}q^2} = \frac{1}{q^2_{\mathrm{max}} - q^2_{\mathrm{min}}} \frac{N_{\mathrm{sig}}}{N_{J/\psi\,\phi}} \frac{\epsilon_{J/\psi\,\phi}}{\epsilon_{\phi\mu^+\mu^-}} \mathcal{B}(B_s^0 \to J/\psi\,\phi)\mathcal{B}(J/\psi \to \mu^+\mu^-), \qquad (4.1)$$

where N_{sig} and $N_{J/\psi\,\phi}$ denote the yields of the $B_s^0 \to \phi\mu^+\mu^-$ and $B_s^0 \to J/\psi\,\phi$ candidates and $\epsilon_{\phi\mu^+\mu^-}$ and $\epsilon_{J/\psi\,\phi}$ denote their respective efficiencies. Since the reconstruction and selection efficiency of the signal decay depends on q^2, a separate efficiency ratio $\epsilon_{J/\psi\,\phi}/\epsilon_{\phi\mu^+\mu^-}$ is determined for every q^2 bin. The branching fractions used in eq. (4.1) are given by $\mathcal{B}(B_s^0 \to J/\psi\,\phi) = (10.50 \pm 1.05) \times 10^{-4}$ [16] and $\mathcal{B}(J/\psi \to \mu^+\mu^-) = (5.93 \pm 0.06) \times 10^{-2}$ [12]. The resulting q^2-dependent differential branching fraction $\mathrm{d}\mathcal{B}(B_s^0 \to \phi\mu^+\mu^-)/\mathrm{d}q^2$ is shown in figure 3. Possible contributions from B_s^0 decays to $K^+K^-\mu^+\mu^-$, with the K^+K^- pair in

JHEP07(2013)084

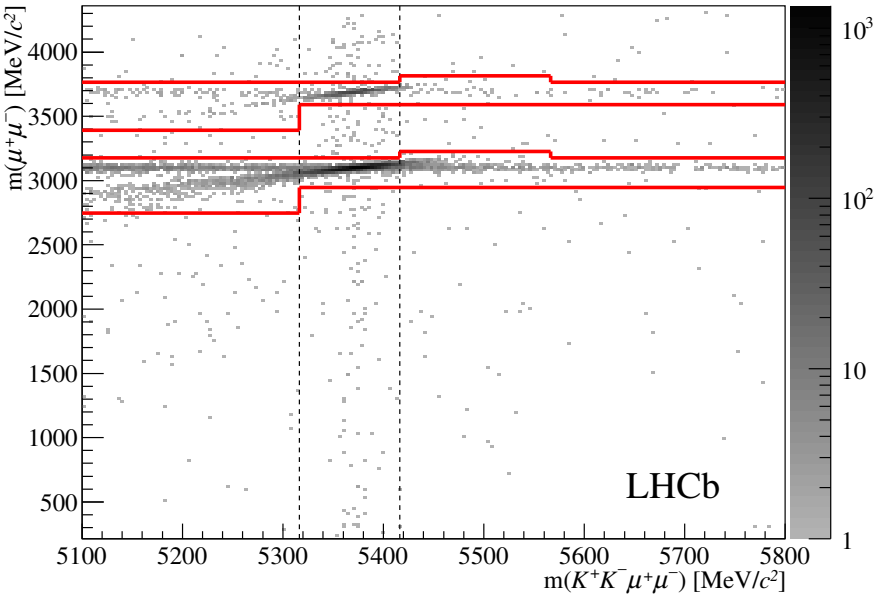

Figure 1. Invariant $\mu^+\mu^-$ versus $K^+K^-\mu^+\mu^-$ mass. The charmonium vetoes are indicated by the solid lines. The vertical dashed lines indicate the signal region of $\pm 50\,\mathrm{MeV}/c^2$ around the known B_s^0 mass in which the signal decay $B_s^0 \to \phi\mu^+\mu^-$ is visible.

q^2 bin (GeV^2/c^4)	N_{sig}	$\mathrm{d}\mathcal{B}/\mathrm{d}q^2$ ($10^{-8}\,\mathrm{GeV}^{-2}c^4$)
$0.10 < q^2 < 2.00$	$25.0\,^{+5.8}_{-5.2}$	$4.72\,^{+1.09}_{-0.98} \pm 0.20 \pm 0.47$
$2.00 < q^2 < 4.30$	$14.3\,^{+4.9}_{-4.3}$	$2.30\,^{+0.79}_{-0.69} \pm 0.11 \pm 0.23$
$4.30 < q^2 < 8.68$	$41.2\,^{+7.5}_{-7.0}$	$3.15\,^{+0.58}_{-0.53} \pm 0.12 \pm 0.31$
$10.09 < q^2 < 12.90$	$40.7\,^{+7.7}_{-7.2}$	$4.26\,^{+0.81}_{-0.75} \pm 0.26 \pm 0.43$
$14.18 < q^2 < 16.00$	$23.8\,^{+5.9}_{-5.3}$	$4.17\,^{+1.04}_{-0.93} \pm 0.24 \pm 0.42$
$16.00 < q^2 < 19.00$	$26.6\,^{+5.7}_{-5.3}$	$3.52\,^{+0.76}_{-0.70} \pm 0.20 \pm 0.35$
$1.00 < q^2 < 6.00$	$31.4\,^{+7.0}_{-6.3}$	$2.27\,^{+0.50}_{-0.46} \pm 0.11 \pm 0.23$

Table 1. Signal yield and differential branching fraction $\mathrm{d}\mathcal{B}(B_s^0 \to \phi\mu^+\mu^-)/\mathrm{d}q^2$ in six bins of q^2. Results are also quoted for the region $1 < q^2 < 6\,\mathrm{GeV}/c^2$ where theoretical predictions are most reliable. The first uncertainty is statistical, the second systematic, and the third from the branching fraction of the normalisation channel.

an S-wave configuration, are neglected in this analysis. The S-wave fraction is expected to be small, for the decay $B_s^0 \to J/\psi K^+K^-$ it is measured to be $(1.1 \pm 0.1\,^{+0.2}_{-0.1})\%$ [16] for the K^+K^- mass window used in this analysis.

The total branching fraction is determined by summing the differential branching fractions in the six q^2 bins. Using the form factor calculations described in ref. [17] the signal fraction rejected by the charmonium vetoes is determined to be 17.7%. This number is confirmed by a different form factor calculation detailed in ref. [18]. No uncertainty is assigned to the vetoed signal fraction. Correcting for the charmonium vetoes, the branching

JHEP07(2013)084

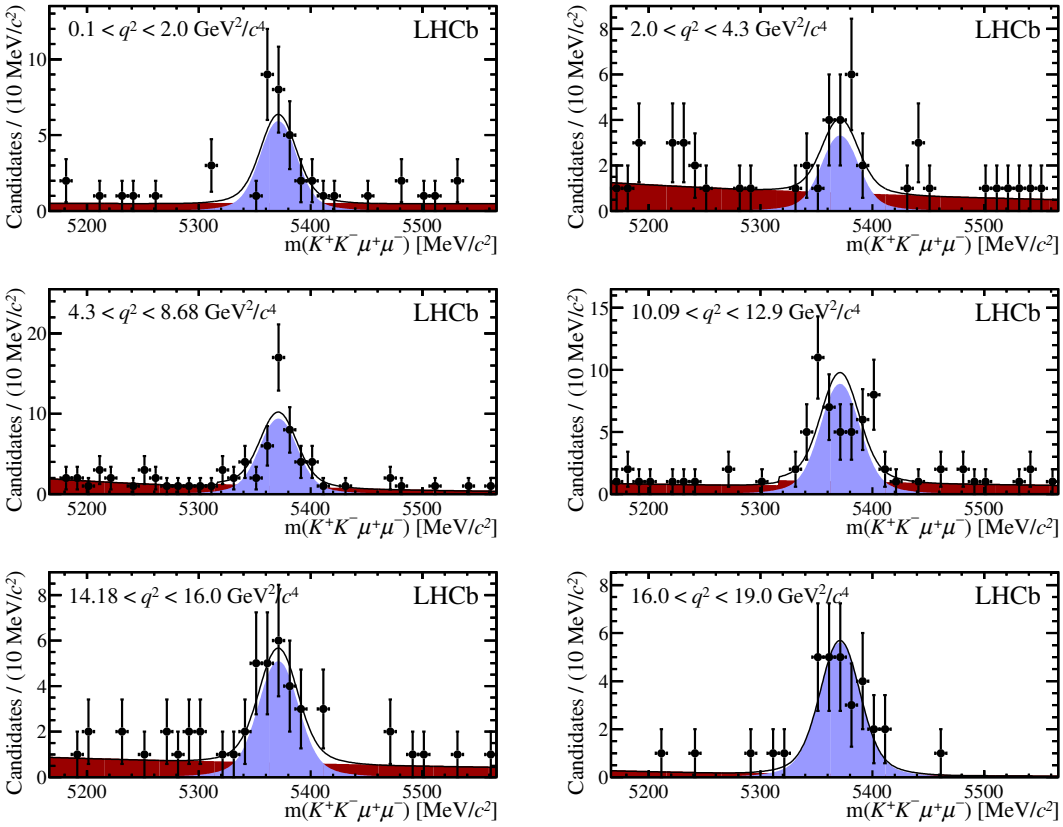

Figure 2. Invariant mass of $B_s^0 \to \phi\mu^+\mu^-$ candidates in six bins of invariant dimuon mass squared. The fitted signal component is denoted by the light blue shaded area, the combinatorial background component by the dark red shaded area. The solid line indicates the sum of the signal and background components.

fraction ratio $\mathcal{B}\left(B_s^0 \to \phi\mu^+\mu^-\right)/\mathcal{B}\left(B_s^0 \to J/\psi\,\phi\right)$ is measured to be

$$\frac{\mathcal{B}(B_s^0 \to \phi\mu^+\mu^-)}{\mathcal{B}(B_s^0 \to J/\psi\,\phi)} = \left(6.74\,^{+0.61}_{-0.56} \pm 0.16\right) \times 10^{-4}.$$

The systematic uncertainties will be discussed in detail in section 4.1. Using the known branching fraction of the normalisation channel the total branching fraction is

$$\mathcal{B}(B_s^0 \to \phi\mu^+\mu^-) = \left(7.07\,^{+0.64}_{-0.59} \pm 0.17 \pm 0.71\right) \times 10^{-7},$$

where the first uncertainty is statistical, the second systematic and the third from the uncertainty on the branching fraction of the normalisation channel.

4.1 Systematic uncertainties on the differential branching fraction

The dominant source of systematic uncertainty on the differential branching fraction arises from the uncertainty on the branching fraction of the normalisation channel $B_s^0 \to J/\psi\,\phi$ ($J/\psi \to \mu^+\mu^-$), which is known to an accuracy of 10% [16]. This uncertainty is fully correlated between all q^2 bins.

JHEP07(2013)084

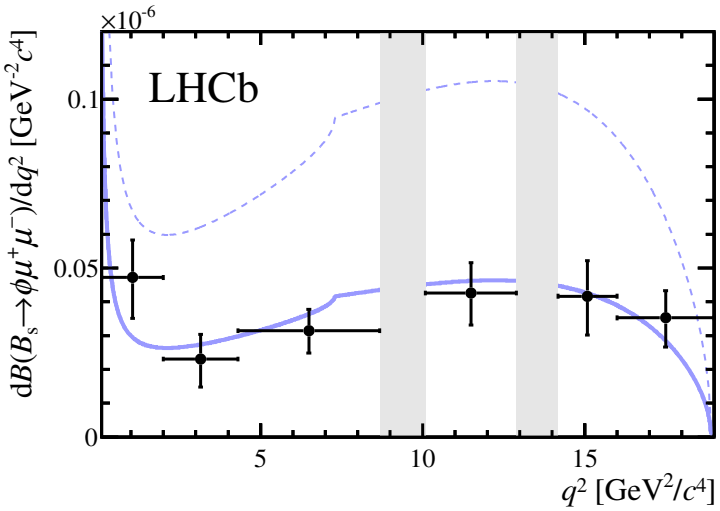

Figure 3. Differential branching fraction $\mathrm{d}\mathcal{B}(B_s^0 \to \phi\mu^+\mu^-)/\mathrm{d}q^2$. Error bars include both statistical and systematic uncertainties added in quadrature. Shaded areas indicate the vetoed regions containing the J/ψ and $\psi(2S)$ resonances. The solid curve shows the leading order SM prediction, scaled to the fitted total branching fraction. The prediction uses the SM Wilson coefficients and leading order amplitudes given in ref. [2], as well as the form factor calculations in ref. [17]. B_s^0 mixing is included as described in ref. [1]. No error band is given for the theory prediction. The dashed curve denotes the leading order prediction scaled to a total branching fraction of 16×10^{-7} [19].

Many of the systematic uncertainties affect the relative efficiencies $\epsilon_{J/\psi\phi}/\epsilon_{\phi\mu^+\mu^-}$ that are determined using simulation. The limited size of the simulated samples causes an uncertainty of $\sim 1\%$ on the ratio in each bin. Simulated events are corrected for known discrepancies between simulation and data. The systematic uncertainties associated with these corrections (*e.g.* tracking efficiency and performance of the particle identification) are typically of the order of 1–2%. The correction procedure for the impact parameter resolution has an effect of up to 5%. Averaging the relative efficiency within the q^2 bins leads to a systematic uncertainty of 1–2%. Other systematic uncertainties of the same magnitude include the trigger efficiency and the uncertainties of the angular distributions of the signal decay $B_s^0 \to \phi\mu^+\mu^-$. The influence of the signal mass shape is found to be 0.5%. The background shape has an effect of up to 5%, which is evaluated by using a linear function to describe the mass distribution of the background instead of the nominal exponential shape. Peaking backgrounds cause a systematic uncertainty of 1–2% on the differential branching fraction. The size of the systematics uncertainties on the differential branching fraction, added in quadrature, ranges from 4–6%. This is small compared to the dominant systematic uncertainty of 10% due to the branching fraction of the normalisation channel, which is given separately in table 1, and the statistical uncertainty.

5 Angular analysis

The angular observables F_{L}, S_3, A_6, and A_9 are determined using unbinned maximum likelihood fits to the distributions of $\cos\theta_K$, $\cos\theta_\ell$, Φ, and the invariant mass of the $K^+K^-\mu^+\mu^-$

JHEP07(2013)084

system. The detector acceptance and the reconstruction and selection of the signal decay distort the angular distributions given in eqs. (1.2)–(1.4). To account for this angular acceptance effect, an angle-dependent efficiency is introduced that factorises in $\cos\theta_K$ and $\cos\theta_\ell$, and is independent of the angle Φ, *i.e.* $\epsilon(\cos\theta_K, \cos\theta_\ell, \Phi) = \epsilon_K(\cos\theta_K) \cdot \epsilon_\ell(\cos\theta_\ell)$. The factors $\epsilon_K(\cos\theta_K)$ and $\epsilon_\ell(\cos\theta_\ell)$ are determined from fits to simulated events. Even Chebyshev polynomial functions of up to fourth order are used to parametrise $\epsilon_K(\cos\theta_K)$ and $\epsilon_\ell(\cos\theta_\ell)$ for each bin of q^2. The point-to-point dissimilarity method described in ref. [20] confirms that the angular acceptance effect is well described by the acceptance model.

Taking the acceptances into account and integrating eq. (1.1) over two angles, results in

$$\frac{1}{\mathrm{d}\Gamma/\mathrm{d}q^2}\frac{\mathrm{d}^2\Gamma}{\mathrm{d}q^2\,\mathrm{d}\cos\theta_K} = \epsilon_K(\cos\theta_K)\left[\frac{3}{4}(1-F_\mathrm{L})(1-\cos^2\theta_K)\,\xi_1 + \frac{3}{2}F_\mathrm{L}\cos^2\theta_K\,\xi_2\right], \tag{5.1}$$

$$\frac{1}{\mathrm{d}\Gamma/\mathrm{d}q^2}\frac{\mathrm{d}^2\Gamma}{\mathrm{d}q^2\,\mathrm{d}\cos\theta_\ell} = \epsilon_\ell(\cos\theta_\ell)\left[\frac{3}{8}(1-F_\mathrm{L})(1+\cos^2\theta_\ell)\,\xi_3 + \frac{3}{4}F_\mathrm{L}(1-\cos^2\theta_\ell)\,\xi_4 + \frac{3}{4}A_6\cos\theta_\ell\,\xi_3\right], \tag{5.2}$$

$$\frac{1}{\mathrm{d}\Gamma/\mathrm{d}q^2}\frac{\mathrm{d}^2\Gamma}{\mathrm{d}q^2\,\mathrm{d}\Phi} = \left[\frac{1}{2\pi}\xi_1\xi_3 + \frac{1}{2\pi}F_\mathrm{L}(\xi_2\xi_4 - \xi_1\xi_3) + \frac{1}{2\pi}S_3\cos 2\Phi\,\xi_2\xi_3 + \frac{1}{2\pi}A_9\sin 2\Phi\,\xi_2\xi_3\right]. \tag{5.3}$$

The terms ξ_i are correction factors with respect to eqs. (1.2)–(1.4) and are given by the angular integrals

$$\begin{aligned}
\xi_1 &= \frac{3}{8}\int_{-1}^{+1}(1+\cos^2\theta_\ell)\epsilon_\ell(\cos\theta_\ell)\mathrm{d}\cos\theta_\ell,\\
\xi_2 &= \frac{3}{4}\int_{-1}^{+1}(1-\cos^2\theta_\ell)\epsilon_\ell(\cos\theta_\ell)\mathrm{d}\cos\theta_\ell,\\
\xi_3 &= \frac{3}{4}\int_{-1}^{+1}(1-\cos^2\theta_K)\epsilon_K(\cos\theta_K)\mathrm{d}\cos\theta_K,\\
\xi_4 &= \frac{3}{2}\int_{-1}^{+1}\cos^2\theta_K\epsilon_K(\cos\theta_K)\mathrm{d}\cos\theta_K.
\end{aligned} \tag{5.4}$$

Three two-dimensional maximum likelihood fits in the decay angles and the reconstructed B_s^0 mass are performed for each q^2 bin to determine the angular observables. The observable F_L is determined in the fit to the $\cos\theta_K$ distribution described by eq. (5.1). The $\cos\theta_\ell$ distribution given by eq. (5.2) is used to determine A_6. Both S_3 and A_9 are measured from the Φ distribution, as described by eq. (5.3). In the fit of the Φ distribution a Gaussian constraint is applied to the parameter F_L using the value of F_L determined from the $\cos\theta_K$ distribution. The constraint on F_L has negligible influence on the values of S_3 and A_9. The angular distribution of the background events is fit using Chebyshev polynomial functions of second order. The mass shapes of the signal and background are described by the sum of two Gaussian distributions with a common mean, and an exponential function, respectively. The effect of the veto of the radiative tails on the combinatorial background is accounted for by using an appropriate scale factor.

JHEP07(2013)084

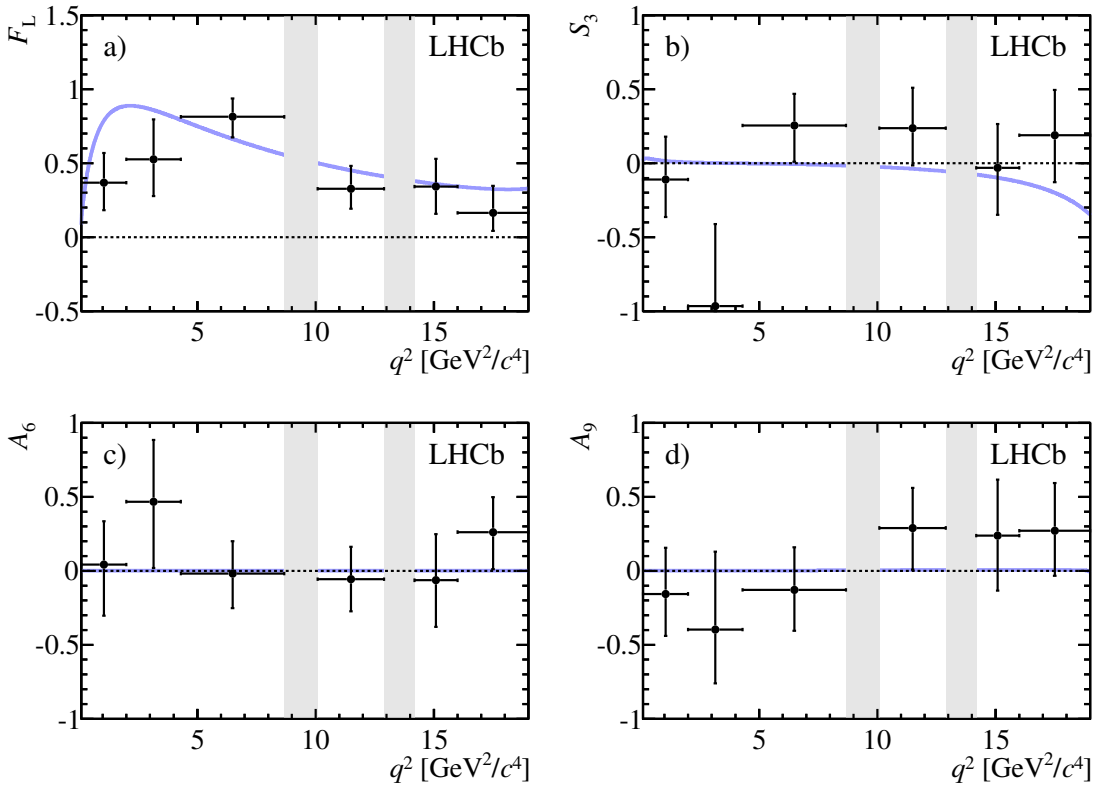

Figure 4. a) Longitudinal polarisation fraction $F_{\rm L}$, b) S_3, c) A_6, and d) A_9 in six bins of q^2. Error bars include statistical and systematic uncertainties added in quadrature. The solid curves are the leading order SM predictions, using the Wilson coefficients and leading order amplitudes given in ref. [2], as well as the form factor calculations in ref. [17]. B^0_s mixing is included as described in ref. [1]. No error band is given for the theory predictions.

q^2 bin (GeV^2/c^4)	$F_{\rm L}$	S_3	A_6	A_9
$0.10 < q^2 < 2.00$	$0.37\,^{+0.19}_{-0.17} \pm 0.07$	$-0.11\,^{+0.28}_{-0.25} \pm 0.05$	$0.04\,^{+0.27}_{-0.32} \pm 0.12$	$-0.16\,^{+0.30}_{-0.27} \pm 0.09$
$2.00 < q^2 < 4.30$	$0.53\,^{+0.25}_{-0.23} \pm 0.10$	$-0.97\,^{+0.53}_{-0.03} \pm 0.17$	$0.47\,^{+0.39}_{-0.42} \pm 0.14$	$-0.40\,^{+0.52}_{-0.35} \pm 0.11$
$4.30 < q^2 < 8.68$	$0.81\,^{+0.11}_{-0.13} \pm 0.05$	$0.25\,^{+0.21}_{-0.24} \pm 0.05$	$-0.02\,^{+0.20}_{-0.21} \pm 0.10$	$-0.13\,^{+0.27}_{-0.26} \pm 0.10$
$10.09 < q^2 < 12.90$	$0.33\,^{+0.14}_{-0.12} \pm 0.06$	$0.24\,^{+0.27}_{-0.25} \pm 0.06$	$-0.06\,^{+0.20}_{-0.20} \pm 0.08$	$0.29\,^{+0.25}_{-0.26} \pm 0.10$
$14.18 < q^2 < 16.00$	$0.34\,^{+0.18}_{-0.17} \pm 0.07$	$-0.03\,^{+0.29}_{-0.31} \pm 0.06$	$-0.06\,^{+0.30}_{-0.30} \pm 0.08$	$0.24\,^{+0.36}_{-0.35} \pm 0.12$
$16.00 < q^2 < 19.00$	$0.16\,^{+0.17}_{-0.10} \pm 0.07$	$0.19\,^{+0.30}_{-0.31} \pm 0.05$	$0.26\,^{+0.22}_{-0.24} \pm 0.08$	$0.27\,^{+0.31}_{-0.28} \pm 0.11$
$1.00 < q^2 < 6.00$	$0.56\,^{+0.17}_{-0.16} \pm 0.09$	$-0.21\,^{+0.24}_{-0.22} \pm 0.08$	$0.20\,^{+0.29}_{-0.27} \pm 0.07$	$-0.30\,^{+0.30}_{-0.29} \pm 0.11$

Table 2. Results for the angular observables $F_{\rm L}$, S_3, A_6, and A_9 in bins of q^2. The first uncertainty is statistical, the second systematic.

The measured angular observables are presented in figure 4 and table 2. The 68% confidence intervals are determined using the Feldman-Cousins method [21] and the nuisance parameters are included using the plug-in method [22].

JHEP07(2013)084

5.1 Systematic uncertainties on the angular observables

The dominant systematic uncertainty on the angular observables is due to the angular acceptance model. Using the point-to-point dissimilarity method detailed in ref. [20], the acceptance model is shown to describe the angular acceptance effect for simulated events at the level of 10%. A cross-check of the angular acceptance using the normalisation channel $B_s^0 \to J/\psi\,\phi$ shows good agreement of the angular observables with the values determined in refs. [23] and [24]. For the determination of the systematic uncertainty due to the angular acceptance model, variations of the acceptance curves are used that have the largest impact on the angular observables. The resulting systematic uncertainty is of the order of 0.05–0.10, depending on the q^2 bin.

The limited amount of simulated events accounts for a systematic uncertainty of up to 0.02. The simulation correction procedure (for tracking efficiency, impact parameter resolution, and particle identification performance) has negligible effect on the angular observables. The description of the signal mass shape leads to a negligible systematic uncertainty. The background mass model causes an uncertainty of less than 0.02. The model of the angular distribution of the background can have a large effect since the statistical precision of the background sample is limited. To estimate the effect, the parameters describing the background angular distribution are determined in the high B_s^0 mass sideband ($5416 < m(K^+K^-\mu^+\mu^-) < 5566\,\mathrm{MeV}/c^2$) using a relaxed requirement on the ϕ mass. The effect is typically 0.05–0.10. Peaking backgrounds cause systematic deviations of the order of 0.01–0.02. Due to the sizeable lifetime difference in the B_s^0 system [24] a decay time dependent acceptance can in principle affect the angular observables. The deviation of the observables due to this effect is studied and found to be negligible. The total systematic uncertainties, evaluated by adding all components in quadrature, are small compared to the statistical uncertainties.

6 Conclusions

The differential branching fraction of the FCNC decay $B_s^0 \to \phi\mu^+\mu^-$ has been determined. The results are summarised in figure 3 and in table 1. Using the form factor calculations in ref. [17] to determine the fraction of events removed by the charmonium vetoes, the relative branching fraction $\mathcal{B}(B_s^0 \to \phi\mu^+\mu^-)/\mathcal{B}(B_s^0 \to J/\psi\,\phi)$ is determined to be

$$\frac{\mathcal{B}(B_s^0 \to \phi\mu^+\mu^-)}{\mathcal{B}(B_s^0 \to J/\psi\,\phi)} = \left(6.74\,^{+0.61}_{-0.56} \pm 0.16\right) \times 10^{-4}.$$

This value is compatible with a previous measurement by the CDF collaboration of $\mathcal{B}(B_s^0 \to \phi\mu^+\mu^-)/\mathcal{B}(B_s^0 \to J/\psi\,\phi) = (11.3 \pm 1.9 \pm 0.7) \times 10^{-4}$ [25] and a recent preliminary result which yields $\mathcal{B}(B_s^0 \to \phi\mu^+\mu^-)/\mathcal{B}(B_s^0 \to J/\psi\,\phi) = (9.0 \pm 1.4 \pm 0.7) \times 10^{-4}$ [26]. Using the branching fraction of the normalisation channel, $\mathcal{B}(B_s^0 \to J/\psi\,\phi) = (10.50 \pm 1.05) \times 10^{-4}$ [16], the total branching fraction of the decay is determined to be

$$\mathcal{B}(B_s^0 \to \phi\mu^+\mu^-) = \left(7.07\,^{+0.64}_{-0.59} \pm 0.17 \pm 0.71\right) \times 10^{-7},$$

JHEP07(2013)084

where the first uncertainty is statistical, the second systematic, and the third from the uncertainty of the branching fraction of the normalisation channel. This measurement constitutes the most precise determination of the $B_s^0 \to \phi\mu^+\mu^-$ branching fraction to date. The measured value is lower than the SM theory predictions that range from 14.5×10^{-7} to 19.2×10^{-7} [19, 27–29]. The uncertainties on these predictions originating from the form factor calculations are typically of the order of 20–30%.

In addition, the first angular analysis of the decay $B_s^0 \to \phi\mu^+\mu^-$ has been performed. The angular observables $F_{\rm L}$, S_3, A_6, and A_9 are determined in bins of q^2, using the distributions of $\cos\theta_K$, $\cos\theta_\ell$, and Φ. The results are summarised in figure 4, and the numerical values are given in table 2. All measured angular observables are consistent with the leading order SM expectation.

Acknowledgments

We express our gratitude to our colleagues in the CERN accelerator departments for the excellent performance of the LHC. We thank the technical and administrative staff at the LHCb institutes. We acknowledge support from CERN and from the national agencies: CAPES, CNPq, FAPERJ and FINEP (Brazil); NSFC (China); CNRS/IN2P3 and Region Auvergne (France); BMBF, DFG, HGF and MPG (Germany); SFI (Ireland); INFN (Italy); FOM and NWO (The Netherlands); SCSR (Poland); ANCS/IFA (Romania); MinES, Rosatom, RFBR and NRC "Kurchatov Institute" (Russia); MinECo, XuntaGal and GENCAT (Spain); SNSF and SER (Switzerland); NAS Ukraine (Ukraine); STFC (United Kingdom); NSF (USA). We also acknowledge the support received from the ERC under FP7. The Tier1 computing centres are supported by IN2P3 (France), KIT and BMBF (Germany), INFN (Italy), NWO and SURF (The Netherlands), PIC (Spain), GridPP (United Kingdom). We are thankful for the computing resources put at our disposal by Yandex LLC (Russia), as well as to the communities behind the multiple open source software packages that we depend on.

Open Access. This article is distributed under the terms of the Creative Commons Attribution License which permits any use, distribution and reproduction in any medium, provided the original author(s) and source are credited.

References

[1] C. Bobeth, G. Hiller and G. Piranishvili, *CP asymmetries in $\bar{B} \to \bar{K}^*(\to \bar{K}\pi)\bar{\ell}\ell$ and untagged $\bar{B}_s$, $B_s \to \phi(\to K^+K^-)\bar{\ell}\ell$ decays at NLO*, *JHEP* **07** (2008) 106 [arXiv:0805.2525] [INSPIRE].

[2] W. Altmannshofer et al., *Symmetries and asymmetries of $B \to K^*\mu^+\mu^-$ decays in the Standard Model and beyond*, *JHEP* **01** (2009) 019 [arXiv:0811.1214] [INSPIRE].

[3] LHCb collaboration, *The LHCb detector at the LHC*, 2008 *JINST* **3** S08005 [INSPIRE].

[4] R. Aaij et al., *The LHCb trigger and its performance in 2011*, 2013 *JINST* **8** P04022 [arXiv:1211.3055] [INSPIRE].

JHEP07(2013)084

[5] T. Sjöstrand, S. Mrenna and P.Z. Skands, *PYTHIA 6.4 physics and manual*, *JHEP* **05** (2006) 026 [hep-ph/0603175] [INSPIRE].

[6] I. Belyaev et al., *Handling of the generation of primary events in GAUSS, the LHCb simulation framework*, *IEEE Nucl. Sci. Symp. Conf. Rec.* (2010) 1155.

[7] D. Lange, *The EvtGen particle decay simulation package*, *Nucl. Instrum. Meth.* **A 462** (2001) 152 [INSPIRE].

[8] P. Golonka and Z. Was, *PHOTOS Monte Carlo: a precision tool for QED corrections in Z and W decays*, *Eur. Phys. J.* **C 45** (2006) 97 [hep-ph/0506026] [INSPIRE].

[9] GEANT4 collaboration, J. Allison et al., *GEANT4 developments and applications*, *IEEE Trans. Nucl. Sci.* **53** (2006) 270.

[10] GEANT4 collaboration, S. Agostinelli et al., *GEANT4: a simulation toolkit*, *Nucl. Instrum. Meth.* **A 506** (2003) 250 [INSPIRE].

[11] M. Clemencic et al., *The LHCb simulation application, GAUSS: design, evolution and experience*, *J. Phys. Conf. Ser.* **331** (2011) 032023.

[12] Particle Data Group collaboration, J. Beringer et al., *Review of particle physics*, *Phys. Rev.* **D 86** (2012) 010001 [INSPIRE].

[13] L. Breiman, J.H. Friedman, R.A. Olshen and C.J. Stone, *Classification and regression trees*, Wadsworth international group, Belmont U.S.A. (1984).

[14] R.E. Schapire and Y. Freund, *A decision-theoretic generalization of on-line learning and an application to boosting*, *Jour. Comp. and Syst. Sc.* **55** (1997) 119.

[15] LHCb collaboration, *Differential branching fraction and angular analysis of the decay* $B^0 \to K^{*0}\mu^+\mu^-$, arXiv:1304.6325 [INSPIRE].

[16] LHCb collaboration, *Amplitude analysis and the branching fraction measurement of* $\bar{B}^0_s \to J/\psi K^+K^-$, *Phys. Rev.* **D 87** (2013) 072004 [arXiv:1302.1213] [INSPIRE].

[17] P. Ball and R. Zwicky, $B_{d,s} \to \rho, \omega, K^*, \phi$ *decay form-factors from light-cone sum rules revisited*, *Phys. Rev.* **D 71** (2005) 014029 [hep-ph/0412079] [INSPIRE].

[18] A. Ali, E. Lunghi, C. Greub and G. Hiller, *Improved model independent analysis of semileptonic and radiative rare B decays*, *Phys. Rev.* **D 66** (2002) 034002 [hep-ph/0112300] [INSPIRE].

[19] C. Geng and C. Liu, *Study of* $B_s \to (\eta, \eta', \phi)\ell\bar{\ell}$ *decays*, *J. Phys.* **G 29** (2003) 1103 [hep-ph/0303246] [INSPIRE].

[20] M. Williams, *How good are your fits? Unbinned multivariate goodness-of-fit tests in high energy physics*, 2010 *JINST* **5** P09004 [arXiv:1006.3019] [INSPIRE].

[21] G.J. Feldman and R.D. Cousins, *A unified approach to the classical statistical analysis of small signals*, *Phys. Rev.* **D 57** (1998) 3873 [physics/9711021] [INSPIRE].

[22] B. Sen, M. Walker and M. Woodroofe, *On the unified method with nuisance parameters*, *Stat. Sinica* **19** (2009) 301.

[23] CDF collaboration, T. Aaltonen et al., *Measurement of the bottom-strange meson mixing phase in the full CDF data set*, *Phys. Rev. Lett.* **109** (2012) 171802 [arXiv:1208.2967] [INSPIRE].

JHEP07(2013)084

[24] LHCb collaboration, *Measurement of CP violation and the B_s^0 meson decay width difference with $B_s^0 \to J/\psi K^+K^-$ and $B_s^0 \to J/\psi\pi^+\pi^-$ decays*, *Phys. Rev. D 87,* **112010** (2013) [arXiv:1304.2600] [INSPIRE].

[25] CDF collaboration, T. Aaltonen et al., *Observation of the baryonic flavor-changing neutral current decay $\Lambda_b \to \Lambda\mu^+\mu^-$*, *Phys. Rev. Lett.* **107** (2011) 201802 [arXiv:1107.3753] [INSPIRE].

[26] CDF collaboration, T. Aaltonen et al., *Branching ratio measurements of exclusive $b \to s\mu^+\mu^-$ decays and angular analysis in $B^0 \to K^{(*)}\mu^+\mu^-$ decays*, CDF public note 10894 (2012).

[27] G. Erkol and G. Turan, *The exclusive $B_s \to \phi\ell^+\ell^-$ decay in the two Higgs doublet models*, *Eur. Phys. J.* **C 25** (2002) 575 [hep-ph/0203038] [INSPIRE].

[28] U. Yilmaz, *Analysis of $B_s \to \phi\ell^+\ell^-$ decay with new physics effects*, *Eur. Phys. J.* **C 58** (2008) 555 [arXiv:0806.0269] [INSPIRE].

[29] Q. Chang and Y.-H. Gao, *Probe a family non-universal Z' boson effects in $\bar{B}_s \to \phi\mu^+\mu^-$ decay*, *Nucl. Phys.* **B 845** (2011) 179 [arXiv:1101.1272] [INSPIRE].

JHEP07(2013)084

The LHCb collaboration

R. Aaij[40], C. Abellan Beteta[35,n], B. Adeva[36], M. Adinolfi[45], C. Adrover[6], A. Affolder[51], Z. Ajaltouni[5], J. Albrecht[9], F. Alessio[37], M. Alexander[50], S. Ali[40], G. Alkhazov[29], P. Alvarez Cartelle[36], A.A. Alves Jr[24,37], S. Amato[2], S. Amerio[21], Y. Amhis[7], L. Anderlini[17,f], J. Anderson[39], R. Andreassen[56], R.B. Appleby[53], O. Aquines Gutierrez[10], F. Archilli[18], A. Artamonov[34], M. Artuso[58], E. Aslanides[6], G. Auriemma[24,m], S. Bachmann[11], J.J. Back[47], C. Baesso[59], V. Balagura[30], W. Baldini[16], R.J. Barlow[53], C. Barschel[37], S. Barsuk[7], W. Barter[46], Th. Bauer[40], A. Bay[38], J. Beddow[50], F. Bedeschi[22], I. Bediaga[1], S. Belogurov[30], K. Belous[34], I. Belyaev[30], E. Ben-Haim[8], G. Bencivenni[18], S. Benson[49], J. Benton[45], A. Berezhnoy[31], R. Bernet[39], M.-O. Bettler[46], M. van Beuzekom[40], A. Bien[11], S. Bifani[44], T. Bird[53], A. Bizzeti[17,h], P.M. Bjørnstad[53], T. Blake[37], F. Blanc[38], J. Blouw[11], S. Blusk[58], V. Bocci[24], A. Bondar[33], N. Bondar[29], W. Bonivento[15], S. Borghi[53], A. Borgia[58], T.J.V. Bowcock[51], E. Bowen[39], C. Bozzi[16], T. Brambach[9], J. van den Brand[41], J. Bressieux[38], D. Brett[53], M. Britsch[10], T. Britton[58], N.H. Brook[45], H. Brown[51], I. Burducea[28], A. Bursche[39], G. Busetto[21,q], J. Buytaert[37], S. Cadeddu[15], O. Callot[7], M. Calvi[20,j], M. Calvo Gomez[35,n], A. Camboni[35], P. Campana[18,37], D. Campora Perez[37], A. Carbone[14,c], G. Carboni[23,k], R. Cardinale[19,i], A. Cardini[15], H. Carranza-Mejia[49], L. Carson[52], K. Carvalho Akiba[2], G. Casse[51], L. Castillo Garcia[37], M. Cattaneo[37], Ch. Cauet[9], M. Charles[54], Ph. Charpentier[37], P. Chen[3,38], N. Chiapolini[39], M. Chrzaszcz[25], K. Ciba[37], X. Cid Vidal[37], G. Ciezarek[52], P.E.L. Clarke[49], M. Clemencic[37], H.V. Cliff[46], J. Closier[37], C. Coca[28], V. Coco[40], J. Cogan[6], E. Cogneras[5], P. Collins[37], A. Comerma-Montells[35], A. Contu[15,37], A. Cook[45], M. Coombes[45], S. Coquereau[8], G. Corti[37], B. Couturier[37], G.A. Cowan[49], D.C. Craik[47], S. Cunliffe[52], R. Currie[49], C. D'Ambrosio[37], P. David[8], P.N.Y. David[40], A. Davis[56], I. De Bonis[4], K. De Bruyn[40], S. De Capua[53], M. De Cian[39], J.M. De Miranda[1], L. De Paula[2], W. De Silva[56], P. De Simone[18], D. Decamp[4], M. Deckenhoff[9], L. Del Buono[8], N. Déléage[4], D. Derkach[14], O. Deschamps[5], F. Dettori[41], A. Di Canto[11], F. Di Ruscio[23,k], H. Dijkstra[37], M. Dogaru[28], S. Donleavy[51], F. Dordei[11], A. Dosil Suárez[36], D. Dossett[47], A. Dovbnya[42], F. Dupertuis[38], R. Dzhelyadin[34], A. Dziurda[25], A. Dzyuba[29], S. Easo[48,37], U. Egede[52], V. Egorychev[30], S. Eidelman[33], D. van Eijk[40], S. Eisenhardt[49], U. Eitschberger[9], R. Ekelhof[9], L. Eklund[50,37], I. El Rifai[5], Ch. Elsasser[39], D. Elsby[44], A. Falabella[14,e], C. Färber[11], G. Fardell[49], C. Farinelli[40], S. Farry[51], V. Fave[38], D. Ferguson[49], V. Fernandez Albor[36], F. Ferreira Rodrigues[1], M. Ferro-Luzzi[37], S. Filippov[32], M. Fiore[16], C. Fitzpatrick[37], M. Fontana[10], F. Fontanelli[19,i], R. Forty[37], O. Francisco[2], M. Frank[37], C. Frei[37], M. Frosini[17,f], S. Furcas[20], E. Furfaro[23,k], A. Gallas Torreira[36], D. Galli[14,c], M. Gandelman[2], P. Gandini[58], Y. Gao[3], J. Garofoli[58], P. Garosi[53], J. Garra Tico[46], L. Garrido[35], C. Gaspar[37], R. Gauld[54], E. Gersabeck[11], M. Gersabeck[53], T. Gershon[47,37], Ph. Ghez[4], V. Gibson[46], V.V. Gligorov[37], C. Göbel[59], D. Golubkov[30], A. Golutvin[52,30,37], A. Gomes[2], H. Gordon[54], M. Grabalosa Gándara[5], R. Graciani Diaz[35], L.A. Granado Cardoso[37], E. Graugés[35], G. Graziani[17], A. Grecu[28], E. Greening[54], S. Gregson[46], P. Griffith[44], O. Grünberg[60], B. Gui[58], E. Gushchin[32], Yu. Guz[34,37], T. Gys[37], C. Hadjivasiliou[58], G. Haefeli[38], C. Haen[37], S.C. Haines[46], S. Hall[52], T. Hampson[45], S. Hansmann-Menzemer[11], N. Harnew[54], S.T. Harnew[45], J. Harrison[53], T. Hartmann[60], J. He[37], V. Heijne[40], K. Hennessy[51], P. Henrard[5], J.A. Hernando Morata[36], E. van Herwijnen[37], A. Hicheur[1], E. Hicks[51], D. Hill[54], M. Hoballah[5], M. Holtrop[40], C. Hombach[53], P. Hopchev[4], W. Hulsbergen[40], P. Hunt[54], T. Huse[51], N. Hussain[54], D. Hutchcroft[51], D. Hynds[50], V. Iakovenko[43], M. Idzik[26], P. Ilten[12], R. Jacobsson[37], A. Jaeger[11], E. Jans[40], P. Jaton[38], A. Jawahery[57], F. Jing[3], M. John[54], D. Johnson[54], C.R. Jones[46], C. Joram[37], B. Jost[37], M. Kaballo[9], S. Kandybei[42], M. Karacson[37], T.M. Karbach[37], I.R. Kenyon[44], U. Kerzel[37],

JHEP07(2013)084

T. Ketel[41], A. Keune[38], B. Khanji[20], O. Kochebina[7], I. Komarov[38], R.F. Koopman[41], P. Koppenburg[40], M. Korolev[31], A. Kozlinskiy[40], L. Kravchuk[32], K. Kreplin[11], M. Kreps[47], G. Krocker[11], P. Krokovny[33], F. Kruse[9], M. Kucharczyk[20,25,j], V. Kudryavtsev[33], T. Kvaratskheliya[30,37], V.N. La Thi[38], D. Lacarrere[37], G. Lafferty[53], A. Lai[15], D. Lambert[49], R.W. Lambert[41], E. Lanciotti[37], G. Lanfranchi[18], C. Langenbruch[37], T. Latham[47], C. Lazzeroni[44], R. Le Gac[6], J. van Leerdam[40], J.-P. Lees[4], R. Lefèvre[5], A. Leflat[31], J. Lefrançois[7], S. Leo[22], O. Leroy[6], T. Lesiak[25], B. Leverington[11], Y. Li[3], L. Li Gioi[5], M. Liles[51], R. Lindner[37], C. Linn[11], B. Liu[3], G. Liu[37], S. Lohn[37], I. Longstaff[50], J.H. Lopes[2], E. Lopez Asamar[35], N. Lopez-March[38], H. Lu[3], D. Lucchesi[21,q], J. Luisier[38], H. Luo[49], F. Machefert[7], I.V. Machikhiliyan[4,30], F. Maciuc[28], O. Maev[29,37], S. Malde[54], G. Manca[15,d], G. Mancinelli[6], U. Marconi[14], R. Märki[38], J. Marks[11], G. Martellotti[24], A. Martens[8], L. Martin[54], A. Martín Sánchez[7], M. Martinelli[40], D. Martinez Santos[41], D. Martins Tostes[2], A. Massafferri[1], R. Matev[37], Z. Mathe[37], C. Matteuzzi[20], E. Maurice[6], A. Mazurov[16,32,37,e], B. Mc Skelly[51], J. McCarthy[44], A. McNab[53], R. McNulty[12], B. Meadows[56,54], F. Meier[9], M. Meissner[11], M. Merk[40], D.A. Milanes[8], M.-N. Minard[4], J. Molina Rodriguez[59], S. Monteil[5], D. Moran[53], P. Morawski[25], M.J. Morello[22,s], R. Mountain[58], I. Mous[40], F. Muheim[49], K. Müller[39], R. Muresan[28], B. Muryn[26], B. Muster[38], P. Naik[45], T. Nakada[38], R. Nandakumar[48], I. Nasteva[1], M. Needham[49], N. Neufeld[37], A.D. Nguyen[38], T.D. Nguyen[38], C. Nguyen-Mau[38,p], M. Nicol[7], V. Niess[5], R. Niet[9], N. Nikitin[31], T. Nikodem[11], A. Nomerotski[54], A. Novoselov[34], A. Oblakowska-Mucha[26], V. Obraztsov[34], S. Oggero[40], S. Ogilvy[50], O. Okhrimenko[43], R. Oldeman[15,d], M. Orlandea[28], J.M. Otalora Goicochea[2], P. Owen[52], A. Oyanguren[35,o], B.K. Pal[58], A. Palano[13,b], M. Palutan[18], J. Panman[37], A. Papanestis[48], M. Pappagallo[50], C. Parkes[53], C.J. Parkinson[52], G. Passaleva[17], G.D. Patel[51], M. Patel[52], G.N. Patrick[48], C. Patrignani[19,i], C. Pavel-Nicorescu[28], A. Pazos Alvarez[36], A. Pellegrino[40], G. Penso[24,l], M. Pepe Altarelli[37], S. Perazzini[14,c], D.L. Perego[20,j], E. Perez Trigo[36], A. Pérez-Calero Yzquierdo[35], P. Perret[5], M. Perrin-Terrin[6], G. Pessina[20], K. Petridis[52], A. Petrolini[19,i], A. Phan[58], E. Picatoste Olloqui[35], B. Pietrzyk[4], T. Pilař[47], D. Pinci[24], S. Playfer[49], M. Plo Casasus[36], F. Polci[8], G. Polok[25], A. Poluektov[47,33], E. Polycarpo[2], A. Popov[34], D. Popov[10], B. Popovici[28], C. Potterat[35], A. Powell[54], J. Prisciandaro[38], A. Pritchard[51], C. Prouve[7], V. Pugatch[43], A. Puig Navarro[38], G. Punzi[22,r], W. Qian[4], J.H. Rademacker[45], B. Rakotomiaramanana[38], M.S. Rangel[2], I. Raniuk[42], N. Rauschmayr[37], G. Raven[41], S. Redford[54], M.M. Reid[47], A.C. dos Reis[1], S. Ricciardi[48], A. Richards[52], K. Rinnert[51], V. Rives Molina[35], D.A. Roa Romero[5], P. Robbe[7], E. Rodrigues[53], P. Rodriguez Perez[36], S. Roiser[37], V. Romanovsky[34], A. Romero Vidal[36], J. Rouvinet[38], T. Ruf[37], F. Ruffini[22], H. Ruiz[35], P. Ruiz Valls[35,o], G. Sabatino[24,k], J.J. Saborido Silva[36], N. Sagidova[29], P. Sail[50], B. Saitta[15,d], V. Salustino Guimaraes[2], C. Salzmann[39], B. Sanmartin Sedes[36], M. Sannino[19,i], R. Santacesaria[24], C. Santamarina Rios[36], E. Santovetti[23,k], M. Sapunov[6], A. Sarti[18,l], C. Satriano[24,m], A. Satta[23], M. Savrie[16,e], D. Savrina[30,31], P. Schaack[52], M. Schiller[41], H. Schindler[37], M. Schlupp[9], M. Schmelling[10], B. Schmidt[37], O. Schneider[38], A. Schopper[37], M.-H. Schune[7], R. Schwemmer[37], B. Sciascia[18], A. Sciubba[24], M. Seco[36], A. Semennikov[30], K. Senderowska[26], I. Sepp[52], N. Serra[39], J. Serrano[6], P. Seyfert[11], M. Shapkin[34], I. Shapoval[16,42], P. Shatalov[30], Y. Shcheglov[29], T. Shears[51,37], L. Shekhtman[33], O. Shevchenko[42], V. Shevchenko[30], A. Shires[52], R. Silva Coutinho[47], T. Skwarnicki[58], N.A. Smith[51], E. Smith[54,48], M. Smith[53], M.D. Sokoloff[56], F.J.P. Soler[50], F. Soomro[18], D. Souza[45], B. Souza De Paula[2], B. Spaan[9], A. Sparkes[49], P. Spradlin[50], F. Stagni[37], S. Stahl[11], O. Steinkamp[39], S. Stoica[28], S. Stone[58], B. Storaci[39], M. Straticiuc[28], U. Straumann[39], V.K. Subbiah[37], L. Sun[56], S. Swientek[9], V. Syropoulos[41], M. Szczekowski[27], P. Szczypka[38,37], T. Szumlak[26], S. T'Jampens[4], M. Teklishyn[7], E. Teodorescu[28], F. Teubert[37], C. Thomas[54], E. Thomas[37], J. van Tilburg[11], V. Tisserand[4], M. Tobin[38], S. Tolk[41], D. Tonelli[37], S. Topp-Joergensen[54], N. Torr[54],

JHEP07(2013)084

E. Tournefier[4,52], S. Tourneur[38], M.T. Tran[38], M. Tresch[39], A. Tsaregorodtsev[6], P. Tsopelas[40], N. Tuning[40], M. Ubeda Garcia[37], A. Ukleja[27], D. Urner[53], U. Uwer[11], V. Vagnoni[14], G. Valenti[14], R. Vazquez Gomez[35], P. Vazquez Regueiro[36], S. Vecchi[16], J.J. Velthuis[45], M. Veltri[17,g], G. Veneziano[38], M. Vesterinen[37], B. Viaud[7], D. Vieira[2], X. Vilasis-Cardona[35,n], A. Vollhardt[39], D. Volyanskyy[10], D. Voong[45], A. Vorobyev[29], V. Vorobyev[33], C. Voß[60], H. Voss[10], R. Waldi[60], R. Wallace[12], S. Wandernoth[11], J. Wang[58], D.R. Ward[46], N.K. Watson[44], A.D. Webber[53], D. Websdale[52], M. Whitehead[47], J. Wicht[37], J. Wiechczynski[25], D. Wiedner[11], L. Wiggers[40], G. Wilkinson[54], M.P. Williams[47,48], M. Williams[55], F.F. Wilson[48], J. Wishahi[9], M. Witek[25], S.A. Wotton[46], S. Wright[46], S. Wu[3], K. Wyllie[37], Y. Xie[49,37], F. Xing[54], Z. Xing[58], Z. Yang[3], R. Young[49], X. Yuan[3], O. Yushchenko[34], M. Zangoli[14], M. Zavertyaev[10,a], F. Zhang[3], L. Zhang[58], W.C. Zhang[12], Y. Zhang[3], A. Zhelezov[11], A. Zhokhov[30], L. Zhong[3], A. Zvyagin[37]

[1] *Centro Brasileiro de Pesquisas Físicas (CBPF), Rio de Janeiro, Brazil*
[2] *Universidade Federal do Rio de Janeiro (UFRJ), Rio de Janeiro, Brazil*
[3] *Center for High Energy Physics, Tsinghua University, Beijing, China*
[4] *LAPP, Université de Savoie, CNRS/IN2P3, Annecy-Le-Vieux, France*
[5] *Clermont Université, Université Blaise Pascal, CNRS/IN2P3, LPC, Clermont-Ferrand, France*
[6] *CPPM, Aix-Marseille Université, CNRS/IN2P3, Marseille, France*
[7] *LAL, Université Paris-Sud, CNRS/IN2P3, Orsay, France*
[8] *LPNHE, Université Pierre et Marie Curie, Université Paris Diderot, CNRS/IN2P3, Paris, France*
[9] *Fakultät Physik, Technische Universität Dortmund, Dortmund, Germany*
[10] *Max-Planck-Institut für Kernphysik (MPIK), Heidelberg, Germany*
[11] *Physikalisches Institut, Ruprecht-Karls-Universität Heidelberg, Heidelberg, Germany*
[12] *School of Physics, University College Dublin, Dublin, Ireland*
[13] *Sezione INFN di Bari, Bari, Italy*
[14] *Sezione INFN di Bologna, Bologna, Italy*
[15] *Sezione INFN di Cagliari, Cagliari, Italy*
[16] *Sezione INFN di Ferrara, Ferrara, Italy*
[17] *Sezione INFN di Firenze, Firenze, Italy*
[18] *Laboratori Nazionali dell'INFN di Frascati, Frascati, Italy*
[19] *Sezione INFN di Genova, Genova, Italy*
[20] *Sezione INFN di Milano Bicocca, Milano, Italy*
[21] *Sezione INFN di Padova, Padova, Italy*
[22] *Sezione INFN di Pisa, Pisa, Italy*
[23] *Sezione INFN di Roma Tor Vergata, Roma, Italy*
[24] *Sezione INFN di Roma La Sapienza, Roma, Italy*
[25] *Henryk Niewodniczanski Institute of Nuclear Physics Polish Academy of Sciences, Kraków, Poland*
[26] *AGH - University of Science and Technology, Faculty of Physics and Applied Computer Science, Kraków, Poland*
[27] *National Center for Nuclear Research (NCBJ), Warsaw, Poland*
[28] *Horia Hulubei National Institute of Physics and Nuclear Engineering, Bucharest-Magurele, Romania*
[29] *Petersburg Nuclear Physics Institute (PNPI), Gatchina, Russia*
[30] *Institute of Theoretical and Experimental Physics (ITEP), Moscow, Russia*
[31] *Institute of Nuclear Physics, Moscow State University (SINP MSU), Moscow, Russia*
[32] *Institute for Nuclear Research of the Russian Academy of Sciences (INR RAN), Moscow, Russia*
[33] *Budker Institute of Nuclear Physics (SB RAS) and Novosibirsk State University, Novosibirsk, Russia*
[34] *Institute for High Energy Physics (IHEP), Protvino, Russia*
[35] *Universitat de Barcelona, Barcelona, Spain*
[36] *Universidad de Santiago de Compostela, Santiago de Compostela, Spain*

JHEP07(2013)084

[37] European Organization for Nuclear Research (CERN), Geneva, Switzerland
[38] Ecole Polytechnique Fédérale de Lausanne (EPFL), Lausanne, Switzerland
[39] Physik-Institut, Universität Zürich, Zürich, Switzerland
[40] Nikhef National Institute for Subatomic Physics, Amsterdam, The Netherlands
[41] Nikhef National Institute for Subatomic Physics and VU University Amsterdam, Amsterdam, The Netherlands
[42] NSC Kharkiv Institute of Physics and Technology (NSC KIPT), Kharkiv, Ukraine
[43] Institute for Nuclear Research of the National Academy of Sciences (KINR), Kyiv, Ukraine
[44] University of Birmingham, Birmingham, United Kingdom
[45] H.H. Wills Physics Laboratory, University of Bristol, Bristol, United Kingdom
[46] Cavendish Laboratory, University of Cambridge, Cambridge, United Kingdom
[47] Department of Physics, University of Warwick, Coventry, United Kingdom
[48] STFC Rutherford Appleton Laboratory, Didcot, United Kingdom
[49] School of Physics and Astronomy, University of Edinburgh, Edinburgh, United Kingdom
[50] School of Physics and Astronomy, University of Glasgow, Glasgow, United Kingdom
[51] Oliver Lodge Laboratory, University of Liverpool, Liverpool, United Kingdom
[52] Imperial College London, London, United Kingdom
[53] School of Physics and Astronomy, University of Manchester, Manchester, United Kingdom
[54] Department of Physics, University of Oxford, Oxford, United Kingdom
[55] Massachusetts Institute of Technology, Cambridge, MA, United States
[56] University of Cincinnati, Cincinnati, OH, United States
[57] University of Maryland, College Park, MD, United States
[58] Syracuse University, Syracuse, NY, United States
[59] Pontifícia Universidade Católica do Rio de Janeiro (PUC-Rio), Rio de Janeiro, Brazil, associated to[2]
[60] Institut für Physik, Universität Rostock, Rostock, Germany, associated to[11]

[a] P.N. Lebedev Physical Institute, Russian Academy of Science (LPI RAS), Moscow, Russia
[b] Università di Bari, Bari, Italy
[c] Università di Bologna, Bologna, Italy
[d] Università di Cagliari, Cagliari, Italy
[e] Università di Ferrara, Ferrara, Italy
[f] Università di Firenze, Firenze, Italy
[g] Università di Urbino, Urbino, Italy
[h] Università di Modena e Reggio Emilia, Modena, Italy
[i] Università di Genova, Genova, Italy
[j] Università di Milano Bicocca, Milano, Italy
[k] Università di Roma Tor Vergata, Roma, Italy
[l] Università di Roma La Sapienza, Roma, Italy
[m] Università della Basilicata, Potenza, Italy
[n] LIFAELS, La Salle, Universitat Ramon Llull, Barcelona, Spain
[o] IFIC, Universitat de Valencia-CSIC, Valencia, Spain
[p] Hanoi University of Science, Hanoi, Viet Nam
[q] Università di Padova, Padova, Italy
[r] Università di Pisa, Pisa, Italy
[s] Scuola Normale Superiore, Pisa, Italy

JHEP07(2013)084